Impact of Land Surface Initialization Approach on Subseasonal Forecast Skill: A Regional Analysis in the Southern Hemisphere

ANNETTE L. HIRSCH, JATIN KALA, ANDY J. PITMAN, CLAIRE CAROUGE, AND JASON P. EVANS

ARC Centre of Excellence for Climate System Science, and Climate Change Research Centre, University of New South Wales, Sydney, New South Wales, Australia

VANESSA HAVERD

CSIRO Marine and Atmospheric Research, Canberra, Australian Capital Territory, Australia

DAVID MOCKO

SAIC at NASA Goddard Space Flight Center, Greenbelt, Maryland

(Manuscript received 2 January 2013, in final form 6 September 2013)

ABSTRACT

The authors use a sophisticated coupled land–atmosphere modeling system for a Southern Hemisphere subdomain centered over southeastern Australia to evaluate differences in simulation skill from two different land surface initialization approaches. The first approach uses equilibrated land surface states obtained from offline simulations of the land surface model, and the second uses land surface states obtained from reanalyses. The authors find that land surface initialization using prior offline simulations contribute to relative gains in subseasonal forecast skill. In particular, relative gains in forecast skill for temperature of 10%–20% within the first 30 days of the forecast can be attributed to the land surface initialization method using offline states. For precipitation there is no distinct preference for the land surface initialization method, with limited gains in forecast skill irrespective of the lead time. The authors evaluated the asymmetry between maximum and minimum temperatures and found that maximum temperatures had the largest gains in relative forecast skill, exceeding 20% in some regions. These results were statistically significant at the 98% confidence level at up to 60 days into the forecast period. For minimum temperature, using reanalyses to initialize the land surface contributed to relative gains in forecast skill, reaching 40% in parts of the domain that were statistically significant at the 98% confidence level. The contrasting impact of the land surface initialization method between maximum and minimum temperature was associated with different soil moisture coupling mechanisms. Therefore, land surface initialization from prior offline simulations does improve predictability for temperature, particularly maximum temperature, but with less obvious improvements for precipitation and minimum temperature over southeastern Australia.

1. Introduction

In models used for weather forecasting, or climate prediction, soil moisture is a model-specific measure of the wetness in a land surface model (LSM). Various LSMs use different functions to describe soil moisture and can produce different soil moisture climatological means and variability characteristics (Koster et al. 2009). Soil moisture anomalies can affect the atmosphere on short time scales (Beljaars et al. 1996) or on larger time scales (Douville and Chauvin 2000). Fennessy and Shukla (1999) and Douville (2010) have recently demonstrated that seasonal forecasts can benefit from appropriate soil moisture initialization.

The soil moisture feedback on surface climate has been explored through collaborative experiments such as the Global Land–Atmosphere Coupling Experiment (GLACE; Koster et al. 2006, 2011). GLACE is a methodology for using idealized model experiments to explore land–atmosphere coupling. Key research aims

Corresponding author address: Annette L. Hirsch, ARC Centre of Excellence for Climate System Science, Level 4 Mathews Building, University of New South Wales, Kensington, Sydney NSW 2052, Australia.
E-mail: a.hirsch@student.unsw.edu.au

DOI: 10.1175/JHM-D-13-05.1

include quantifying the sensitivity of surface climate to soil moisture anomalies and identifying the persistence of a soil moisture anomaly into a forecast. The second phase of GLACE (GLACE-2) aims to answer the latter question by investigating whether the combination of soil moisture initialization and sufficient memory in the soil water reservoir leads to increased predictability in subseasonal forecasts.

GLACE-2 focused on the Northern Hemisphere. Multiple subseasonal forecasts were run for boreal summer (Koster et al. 2010, 2011; van den Hurk et al. 2012) because the largest impact from soil moisture was anticipated under summer conditions where high net radiation can lead to large fluxes of sensible and latent heat. For North America, multimodel estimates on the change in forecast skill due to land surface initialization show a positive (10%–15%) increase in skill for mean air temperature maintained within the first 16–30 days of the forecast (Koster et al. 2010). These relative gains in skill are maintained over large proportions of North America for up to 46–60 days. For precipitation, gains in forecast skill cover a smaller proportion of North America and are statistically significant less commonly. Koster et al. (2010) also show that the skill varies with the density of the observation network used to create the initial soil moisture fields and that the change in relative forecast skill has some dependence on the magnitude of the soil moisture anomaly at the initialization of the forecast. Larger soil moisture anomalies, whether wet or dry, tend to induce larger changes in the relative skill. In particular, forecasts initialized with an initial soil moisture drier (wetter) than the 10th (90th) percentile contributed to a 25%–35% increase in relative skill for simulations that were maintained over the 60-day forecast.

GLACE-2 results for Europe were examined by van den Hurk et al. (2012). They evaluated the potential predictability defined as the ability of the multimodel ensemble to predict the behavior of a single participating model. Generally, subseasonal forecasts initialized with equilibrated land surface conditions had higher potential predictability relative to those without. Van den Hurk et al. (2012) conduct the same analysis as Koster et al. (2010) for changes in relative forecast skill as a function of lead time. No meaningful change in skill for precipitation was found over Europe, but for mean temperature there were small gains (~5%) in forecast skill. The results for Europe are perhaps less convincing than those for North America, which van den Hurk et al. (2012) attributed to the lower potential predictability of the models over Europe in the GLACE-2 analysis. Van den Hurk et al. (2012) also evaluated whether the relative change in forecast skill is associated with wet or dry soil at forecast initialization but found no significant results for Europe.

While there is some global analysis of GLACE-2 results in Koster et al. (2011), the choice of boreal summer limits the applicability of the results in the Southern Hemisphere. Most of Australia is semiarid and, therefore, water limited; as a consequence, droughts can be sustained over many years (Evans et al. 2011). This contributes to large soil moisture anomalies in space and time that cause the persistence of extreme conditions associated with the soil moisture limitation on surface climate. Indeed, Australia has some of the highest soil evaporation rates in the world, with 64% of evapotranspiration attributable to soil evaporation (Haverd et al. 2012). Given the important role of soil moisture in the Australian climate (Timbal et al. 2002) and the vulnerability of Australia to drought, examining and quantifying land–atmosphere coupling over Australia provides a foundation for future examination of soil moisture variability and its impacts on the Australian climate. For any investigation of land–atmosphere coupling using climate models, it is first necessary to understand the model sensitivity to initialization.

We aim to quantify the sensitivity of forecast skill for the Weather Research and Forecasting Model (WRF; Skamarock et al. 2008) coupled to the Community Atmosphere–Biosphere Land Exchange Model (CABLE; Wang et al. 2011) using two different land surface initialization approaches. The first method includes using equilibrated land surface states obtained from offline CABLE simulations, and the second uses initial states from reanalyses. Both methods have been employed independently (e.g., Santanello et al. 2011; Evans and McCabe 2010), but no comparison of the two methods is available. While the second land surface initialization method differs from the GLACE-2 methodology, the evaluation of land surface initialization methods is GLACE-like and augments the findings of GLACE-2 by illustrating the relative value of the two initialization approaches on forecast skill.

Our analysis expands GLACE-like analyses to consider the impact of land surface initialization on maximum and minimum air temperatures, calculated over the diurnal cycle, to investigate whether there is any asymmetry in the relative change in forecast skill with temperature extrema. This builds on Jaeger and Seneviratne (2011), who explore the impact of soil moisture on climate extremes, again using idealized model simulations to perturb soil moisture content and evaluate the climate sensitivity to these perturbations. By characterizing the change in a number of extremes indices and the distributions of both temperature and precipitation, Jaeger and Seneviratne (2011) characterize the role of soil moisture anomalies for climate extremes and trends. Their analysis is focused on Europe, where soil moisture

was found to have a greater impact in dry conditions. The effect of soil moisture on temperature was found to be asymmetric, with the strongest impact on temperature maxima.

Our study is therefore the first to evaluate the relative value of different land surface initialization methods using the WRF–CABLE combined model. Our aim is to (1) quantify the sensitivities over Australia to land surface initialization, (2) evaluate whether forecast skill has any dependency on wet and dry soil initialization, and (3) evaluate the asymmetry between maximum and minimum temperatures on forecast skill.

2. Methodology

a. Model descriptions

WRF is a community weather and climate model with a nonhydrostatic Eulerian dynamical core with terrain-following, pressure-based vertical coordinates (Skamarock et al. 2008). Commonly used for regional climate modeling, WRF simulations are typically forced with reanalysis at 6-hourly intervals to define the lateral boundary conditions.

In this study, WRF has been coupled to the CABLE LSM. CABLE is a sophisticated LSM that simulates the interactions between microclimate, plant physiology, and hydrology (Wang et al. 2011). CABLE includes a coupled model of stomatal conductance, photosynthesis, and partitioning of absorbed net radiation into latent and sensible heat fluxes. A canopy turbulence model (Raupach et al. 1997) is used to calculate within-canopy air temperatures and humidity. CABLE includes a multilayer soil model with six layers, with the deepest layer at 2.872 m. Soil hydraulic and thermal characteristics depend on the soil type as well as frozen and unfrozen soil moisture content. Each soil type in our model is described by its saturation content with the flow of water parameterized using Darcy's law and the hydraulic conductivity related to soil moisture via the Clapp and Hornberger (1978) relationship. CABLE has been extensively evaluated (Abramowitz et al. 2008; Wang et al. 2011) and has been used to examine local (Abramowitz et al. 2007), regional (Cruz et al. 2010), and global (Zhang et al. 2011; Pitman et al. 2011; de Noblet-Ducoudré et al. 2012) research questions. The model also provides the lower boundary condition for the Australian Community Climate and Earth System Simulator coupled climate model used in global intercomparisons (Kowalczyk et al. 2013).

We use the National Aeronautics and Space Administration (NASA) Land Information System (LIS) version 6.0 to couple CABLE version 1.4 to WRF version 3.2.1. LIS is a software framework for running high-resolution land data assimilation systems that integrate advanced LSMs with high-resolution satellite and in situ observational data to accurately characterize land surface states and fluxes (Kumar et al. 2006). LIS can be used to run an LSM offline or coupled to WRF, making it an ideal tool for running GLACE-2 style model experiments. Within WRF, LIS can be considered as an alternative option to the land surface parameterization. LIS offline simulations require appropriate surface meteorological forcing to solve the governing equations of the soil–vegetation–snow system and predict surface fluxes and soil states. For coupled simulations, LIS–CABLE provides the surface fluxes to WRF, and WRF provides the near-surface temperature, humidity, winds, total precipitation, and shortwave and longwave radiation to LIS–CABLE. LIS–CABLE is treated like other land surface schemes within WRF, with the required forcing fields mapped onto the appropriate model tiles for LIS. Documentation about the LIS software framework can be found in Kumar et al. (2006) and Peters-Lidard et al. (2007).

Within LIS, there are two methods for initializing the land surface for the coupled simulations, either using the results from offline simulations or by obtaining values from a global climate model (GCM) or reanalysis data. The former approach has been employed successfully in Santanello et al. (2011, 2013), and the latter approach is often employed by WRF users, with the first days to months discarded as spinup.

b. Model configuration

The model domain is centered at 32.7°S and 146.1°E on a Lambert projection with a spatial resolution of 50 km (Fig. 1). The size of the domain was selected to limit computational costs with the region including subtropical, temperate, semiarid, desert, and Mediterranean climates (Evans et al. 2011). Thirty atmospheric levels and six soil layers were used with a maximum of five vegetation tiles per grid cell to further resolve the land surface heterogeneity. Although this domain is not global, as in Koster et al. (2010) and van den Hurk et al. (2012), the choice of a smaller domain at a finer-scale resolution enables land surface heterogeneity to be resolved in ways that are currently impractical in global applications.

The selection of the following WRF physics was based on Evans and McCabe (2010). This includes using the WRF Single Moment (WSM) 5-class microphysics scheme, the Rapid Radiative Transfer Model (RRTM) longwave scheme (Mlawer et al. 1997), the Dudhia shortwave scheme (Dudhia 1989), the Yonsei University (YSU) planetary boundary layer scheme (Hong et al.

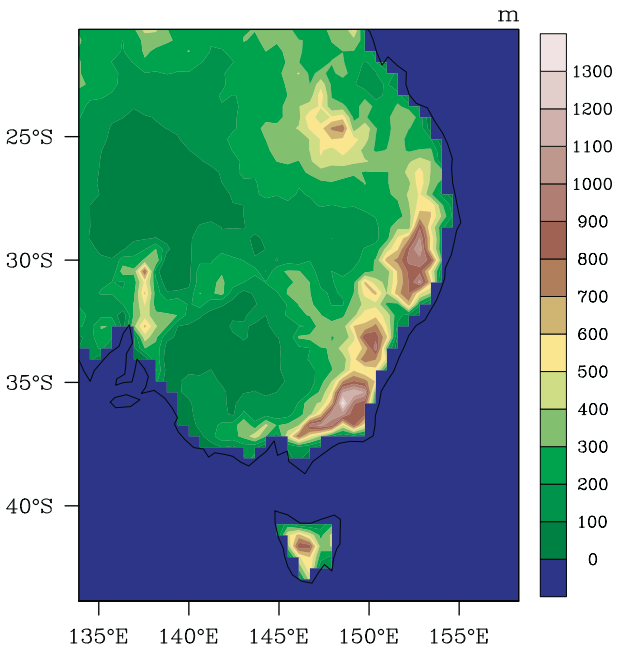

FIG. 1. WRF domain over southeastern Australia at 50 km resolution. Contours correspond to the domain topography height in meters above sea level.

2006), and the Kain–Fritsch cumulus scheme (Kain and Fritsch 1990, 1993; Kain 2004). This configuration has been shown to simulate the regional climate well over time scales ranging from diurnal to interannual (Evans and McCabe 2010; Evans and Westra 2012).

The interim European Centre for Medium-Range Weather Forecasting (ECMWF) Re-Analysis (ERA-Interim) dataset (Dee et al. 2011) was used as the atmospheric initial and boundary conditions for all WRF–LIS–CABLE simulations. ERA-Interim has been used as initial and boundary conditions for WRF in Evans et al. (2012). The Modern-Era Retrospective Analysis for Research and Application (MERRA) land reanalysis was used as the surface meteorological forcing for all offline LIS–CABLE simulations (Reichle et al. 2011). The MERRA data were bias corrected for precipitation using the Australian Bureau of Meteorology (BoM) Australian Water Availability Project (AWAP; Jones et al. 2009) to provide the best possible estimates of the soil moisture state. Details for the bias correction method can be found in Decker et al. (2013).

c. *Experimental design*

We performed two parallel series of 60-day simulations integrated for 10 start dates spaced 15 days apart coincident with Austral summer (e.g., 1 October, 15 October, . . . , 15 February) over 1986–95. This is the same 10-yr period used by Koster et al. (2011), but with the start dates shifted by 6 months. For each unique start date, a 10-member ensemble was run, with ensemble members started 1 day apart.

For the first series (S1), initial land surface states were obtained by running offline LIS–CABLE simulations for 4 yr to obtain equilibrated land surface states for each unique start date. The low computational costs for the offline simulations allowed a consistent procedure for obtaining the initial land surface states. These initial states were examined to ensure spinup had been achieved. This is a ''warm start'' condition where LSM state variables were internally consistent between CABLE and the atmospheric forcing data. The final states from these simulations were then used as the land surface initial conditions for the WRF–LIS–CABLE coupled simulations. The atmospheric initial and boundary conditions are obtained from ERA-Interim. For the second series (S2), all WRF–LIS–CABLE simulations were ''cold starts'' with no prior offline LIS–CABLE simulation to provide the initial land surface states. Instead, these are obtained from ERA-Interim to limit discontinuities to the coupled simulations that might occur if incompatible surface and atmospheric initial conditions were used. Essentially, both series of simulations have an identical configuration, with ERA-Interim used as the atmospheric initial and boundary conditions in both S1 and S2. The only difference between S1 and S2 are the initial land surface conditions for the coupled WRF–LIS–CABLE simulations. We can therefore compare the two different initialization options available for WRF–LIS–CABLE coupled simulations.

Because of limited independent observational datasets to verify the soil moisture estimates in S1 (warm start) and S2 (cold start) and the challenges in comparing observational and modeled estimates of soil moisture (Koster et al. 2009), it is not possible to determine whether one is more realistic than the other. However, the land surface initial conditions in S1 can be considered better than S2 as the spatial structure of the soil moisture and soil temperature fields is well developed in S1 (not shown) and these fields are internally consistent with CABLE.

Given that we use a regional climate model, the simulations are not genuine forecasts as they require information about the large-scale climate from either GCM output or reanalyses. Although our results will be influenced by the lateral boundary conditions, within the domain the regional model develops its own climate. Considering that the lateral boundary forcing is identical for both S1 and S2, any differences between the two series arise from how the land surface was initialized,

and effects from the boundary forcing are very likely minor relative to the contribution from the land surface.

d. Validation datasets

The BoM AWAP version 3 daily gridded precipitation and temperature dataset (Jones et al. 2009) was used for computing relative changes in skill between the model series. AWAP is derived from in situ observations as described in Jones et al. (2009). Daily temperature observations were estimated by averaging the maximum and minimum daily temperatures from AWAP.

A recent review of the AWAP data by King et al. (2013) evaluates the ability of the gridded dataset to capture the rainfall characteristics of high-quality in situ station observations. Although it was found that AWAP tends to underestimate the magnitude of extreme rainfall, the AWAP gridded data closely track station observations, with the exception of regions in central and western Australia, where limited data availability has a large influence. The domain used in this study covers southeastern Australia, where the network density is greatest.

e. Relative skill improvement

For all model output, 15-day averages were computed and then collated across the unique 100 ensemble forecasts to construct time series over December–February (DJF) corresponding to four different lead times over each 60-day ensemble forecast. All analysis is limited to the time series corresponding to the 16–30-, 31–45-, and 46–60-day forecast lead times following Koster et al. (2010, 2011) and van den Hurk et al. (2012). Because of atmospheric initialization, the first lead time corresponding to the 1–15-day average of the ensemble forecasts was discarded as spinup for the coupled model. The same postprocessing was applied to the AWAP data. Following van den Hurk et al. (2012), normalized anomalies were computed by subtracting the time-averaged mean and dividing by the standard deviation. Correlations (R) between the modeled and observed time series were evaluated at each grid cell. The difference between the S1 and the S2 squared correlations (R^2) provides a measure of the contribution of land surface initialization to model skill, with positive (negative) values indicating that using offline simulations (reanalyses) to initialize the land surface produces more skillful forecasts. These diagnostics are similar to those used by Koster et al. (2010, 2011) and van den Hurk et al. (2012). We also extend our analysis to evaluate the impact of land surface initialization on the maximum and minimum air temperatures over the diurnal cycle.

f. Evaluating the impact of extreme soil moisture initialization on relative skill

Following Koster et al. (2010, 2011) and van den Hurk et al. (2012), we evaluate the significance of extreme soil moisture initialization on the relative change in forecast skill between S1 and S2. This required extracting the time series dates corresponding to the extreme upper and lower initial soil moisture anomalies in S1. The identification of extreme soil moisture initialization was based on ranking the vertically integrated soil moisture content from the soil layers within the upper 2 m at each grid point to calculate the upper and lower tercile, quintile, and decile thresholds. Using these thresholds to further split the data, the relative skill improvement was reevaluated at each grid point depending on whether the initial soil moisture in the local area (the 3×3 grid cell region centered on the point in question) exceeded these thresholds or not. By examining the terciles, quintiles, and deciles, we could establish whether the relative skill improvement had a dependence on the magnitude of the extreme initial soil moisture anomaly.

g. Statistical significance

We follow the bootstrapping methodology applied in Koster et al. (2010, 2011) and van den Hurk et al. (2012) to establish the statistical significance of our results. The data are randomly sampled with replacement, and the relative change in skill is calculated from this sample of data. This procedure is repeated 1000 times to obtain 1000 independent estimates of the relative change in skill. If the percentage of positive relative skill estimates exceeds a threshold of $p = 98\%$, then the result is statistically significant. This is the same threshold used by van den Hurk et al. (2012). For regions with negative relative forecast skill, the same hypothesis test can be applied with the statistical significance based upon the percentage of negative relative skill estimates exceeding the same threshold. This technique for establishing statistical significance is computed at each grid cell for each lead time and variable. Figures of this diagnostic for statistical significance contain plots of the percentages based on these estimates and use the same color schemes and scales as in van den Hurk et al. (2012).

3. Results

a. Relative change in forecast skill with lead time

Figure 2 shows our results for southeastern Australia for mean air temperature. The relative gain in forecast skill associated with land surface initialization from offline simulations is regionally variable, with corresponding statistical significance for regions with a larger

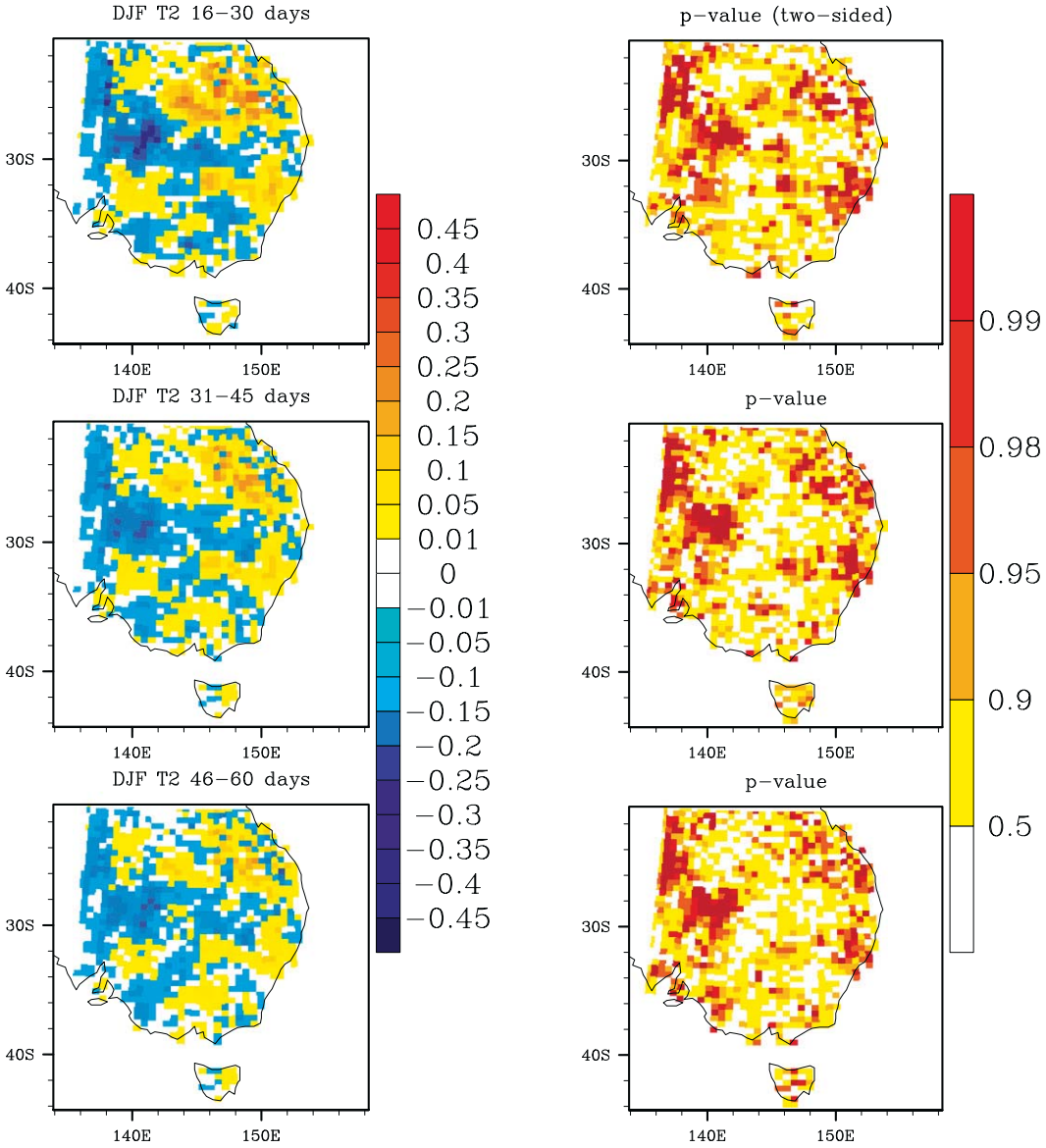

FIG. 2. (left) Relative gain in forecast skill between S1 and S2 for mean 2-m air temperature for three different lead times: (top) 16–30, (middle) 31–45, and (bottom) 46–60 days. Blue (red) regions imply skill of S2 greater (less) than S1. (right) Corresponding *p* value of the difference between S1 and S2 (two sided), where values ≥0.98 indicate that the result is statistically significant using the definition of van den Hurk et al. (2012).

relative change in forecast skill. The northeast quadrant of the domain is associated with a relative gain in S1 forecast skill of 10%–20%. This relative gain is sustained at longer lead times with some reduction in the magnitude, suggesting that at longer lead times the forecast skill converges between the two series as the model integrates forward in time. For the northwest quadrant of the domain, there is a relative loss in S1 skill of 10% that is statistically significant at all lead times. For the southern half of the domain, there are coherent regions with either relative gains or losses in forecast skill that are sustained throughout the 60-day forecasts that are rarely statistically significant at the 95% confidence level, suggesting no preference for land surface initialization method.

The asymmetry in the modeled mean air temperature response to land surface initialization was explored by disaggregating the relative change in forecast skill into contributions from maximum (Fig. 3) and minimum (Fig. 4) air temperature. Maximum temperature has the strongest positive response to land surface initialization using offline simulations. Across most of the domain there are positive relative gains in S1 forecast skill that

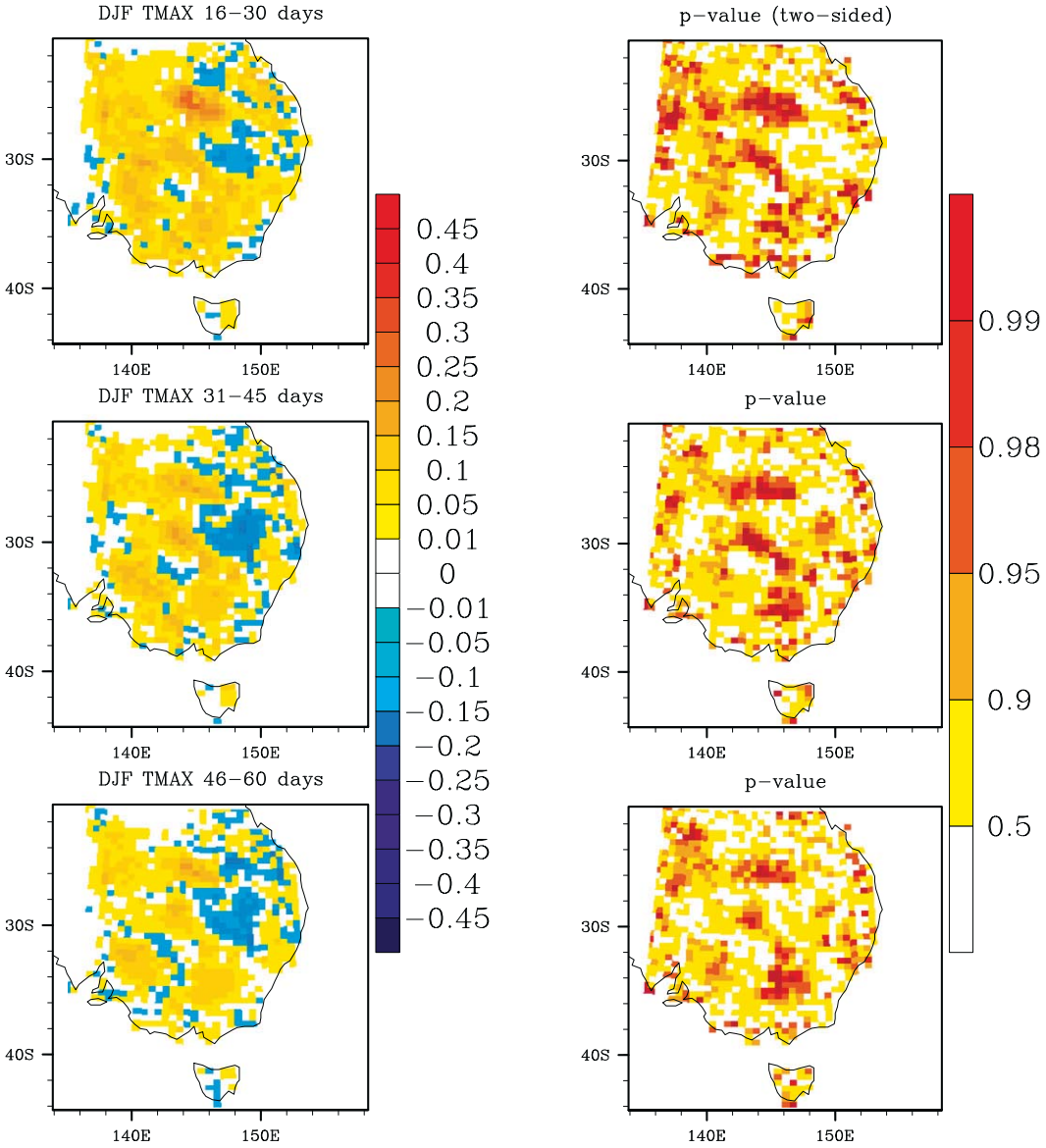

FIG. 3. As in Fig. 2, but for maximum 2-m air temperature.

decrease with lead time. For parts of the domain there are S1 gains reaching with 10%–15% at 16–30 days that decrease to 5%–10% at 60 days into the forecast. In particular, there are some regions where the gain in S1 forecast skill exceeds 20% within the first 30 days of the forecast that are statistically significant at a 98% confidence level. The results for minimum temperature (Fig. 4) strongly resemble those for mean temperature (Fig. 2), particularly for the relative loss (blue regions) in S1 skill across the northwest quadrant of the domain. These negative (blue) regions indicate that land surface initialization from reanalyses (S2) perform better. This feature is sustained across all lead times and is associated with the net radiative response to cloud cover (Fig. 5). Differences in the net shortwave radiation (Fig. 5, top) are small ($<10\,\mathrm{W\,m^{-2}}$) and do not resemble the spatial distribution of the relative skill for minimum temperature in Fig. 4. For net longwave radiation (Fig. 5, middle), S1 has lower values than S2, with larger differences of $\sim 20\,\mathrm{W\,m^{-2}}$ coincident with some of the regions where the negative relative skill for minimum temperature is greatest (Fig. 4). This is particularly evident for the outgoing longwave radiation (Fig. 5, bottom), with differences of $\sim 5\,\mathrm{W\,m^{-2}}$. The response of the downwelling radiation to the land surface initialization can be considered unusual; however, at longer

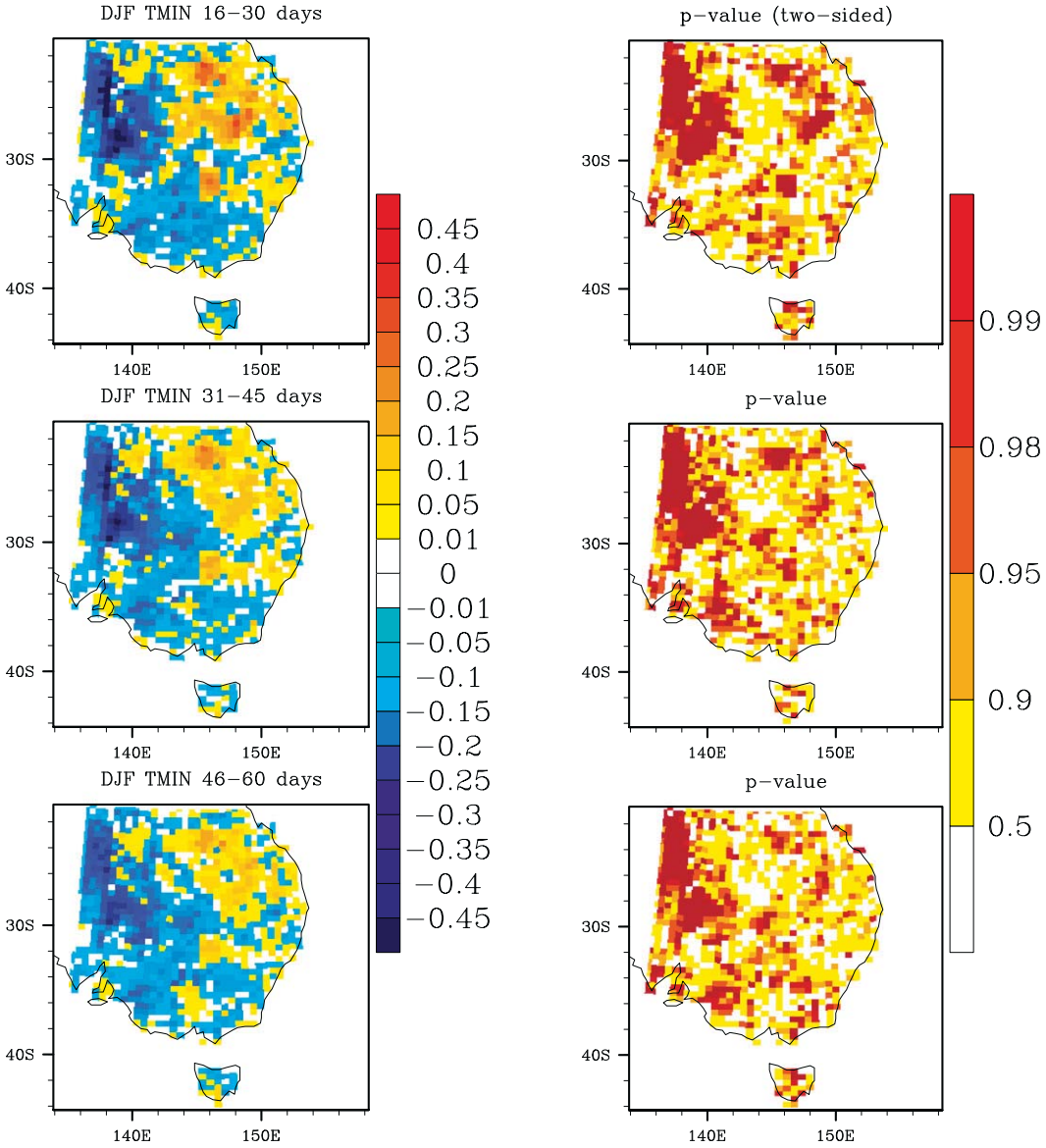

FIG. 4. As in Fig. 2, but for minimum 2-m air temperature.

time scales this difference decreases as the two series converge (not shown). An evaluation of the coupling strength for this configuration of WRF–LIS–CABLE suggests that this model is strongly coupled, with the land surface state exerting a significant influence on the lower boundary condition. Therefore, the strong coupling has implications for the surface energy balance and subsequent land–atmosphere feedbacks on the boundary layer, including the low-level cloud and water vapor that impacts the downwelling radiation. Given the differences in the land surface initialization, the strong coupling of the model can contribute to these differences in the atmosphere initially. As shown in Fig. 2, the two series do converge as the model integrates forward in time, illustrating that the model adjusts to the initial perturbation in the land surface.

To illustrate the asymmetry between maximum and minimum temperatures for the relative change in forecast skill, probability density functions (PDFs) for each lead time are shown in Fig. 6. These PDFs have been constructed using the same dates within DJF used in Figs. 2–4 across all land grid points in the domain. Maximum temperatures tend to have higher relative changes in skill than minimum temperatures (Table 1), which is consistent with the spatial patterns shown in Figs. 3 and 4. This is clear with lead times of 16–30 days,

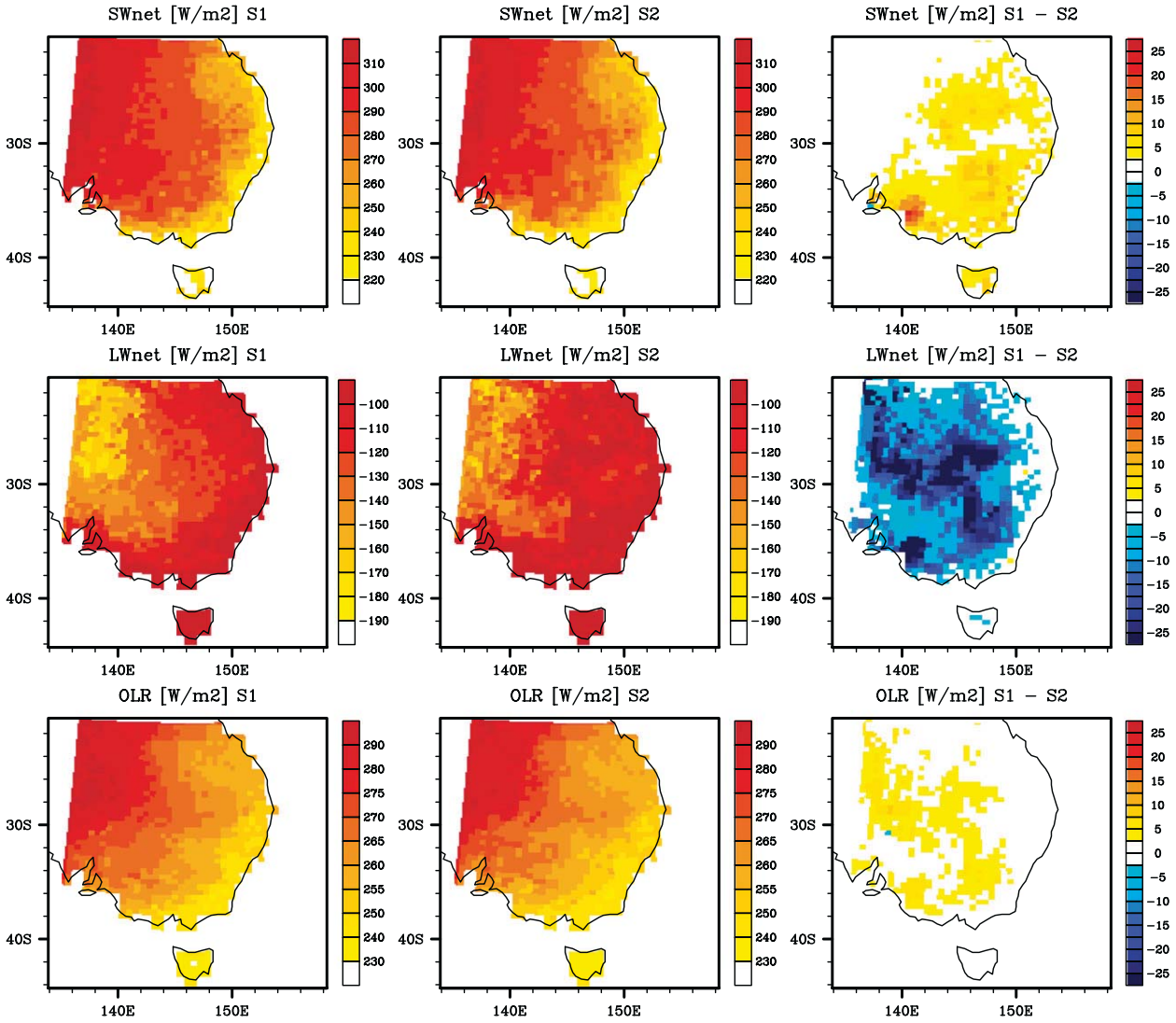

FIG. 5. Comparison of net radiation balance ($W m^{-2}$) between S1 and S2 for the 16–30-day lead time. (left) Temporal mean for S1, (middle) temporal mean for S2, and (right) difference between S1 and S2 temporal means for (top) net shortwave radiation, (middle) net longwave radiation, and (bottom) outgoing longwave radiation. The 31–45- and 46–60-day lead times show similar behavior.

where 79% of the PDF for maximum temperatures is >0.0, indicating an improvement in S1. With subsequent lead times, the PDF is still skewed positive, with 71% and 67% of the PDF > 0 for the 31–45- and 46–60-day lead times, respectively. The relative changes in skill for minimum temperatures have a higher variance. In particular, minimum temperature has a significant low tail at all lead times, with ~60% < 0 at all lead times, indicating S2 performs better. Examining temperature distributions across the domain, S1 is ~2°C warmer than S2 for mean, maximum, and minimum temperatures at all lead times (Fig. 6, right). All temperature distributions are negatively skewed, particularly for maximum temperature, with longer tails for lower temperatures. To understand the systematic warmer temperatures in S1, we examined the sensible heat flux and near-surface soil temperatures. Within the top 1 m, S1 was initialized with soil temperatures warmer than S2 by more than 5°C, with corresponding differences in the sensible heat flux (figure not shown). As the model integrates forward in time, the differences between S1 and S2 soil temperatures decrease at longer lead times but still exceed 2°C at 46–60 days, showing that the forcing soil temperatures are particularly influenced from the model used within the reanalyses. The same spatial patterns are observed for surface air temperatures, with S1 temperatures greater than S2 across most of the domain irrespective of the forecast lead time, which is demonstrated in the temperature PDFs.

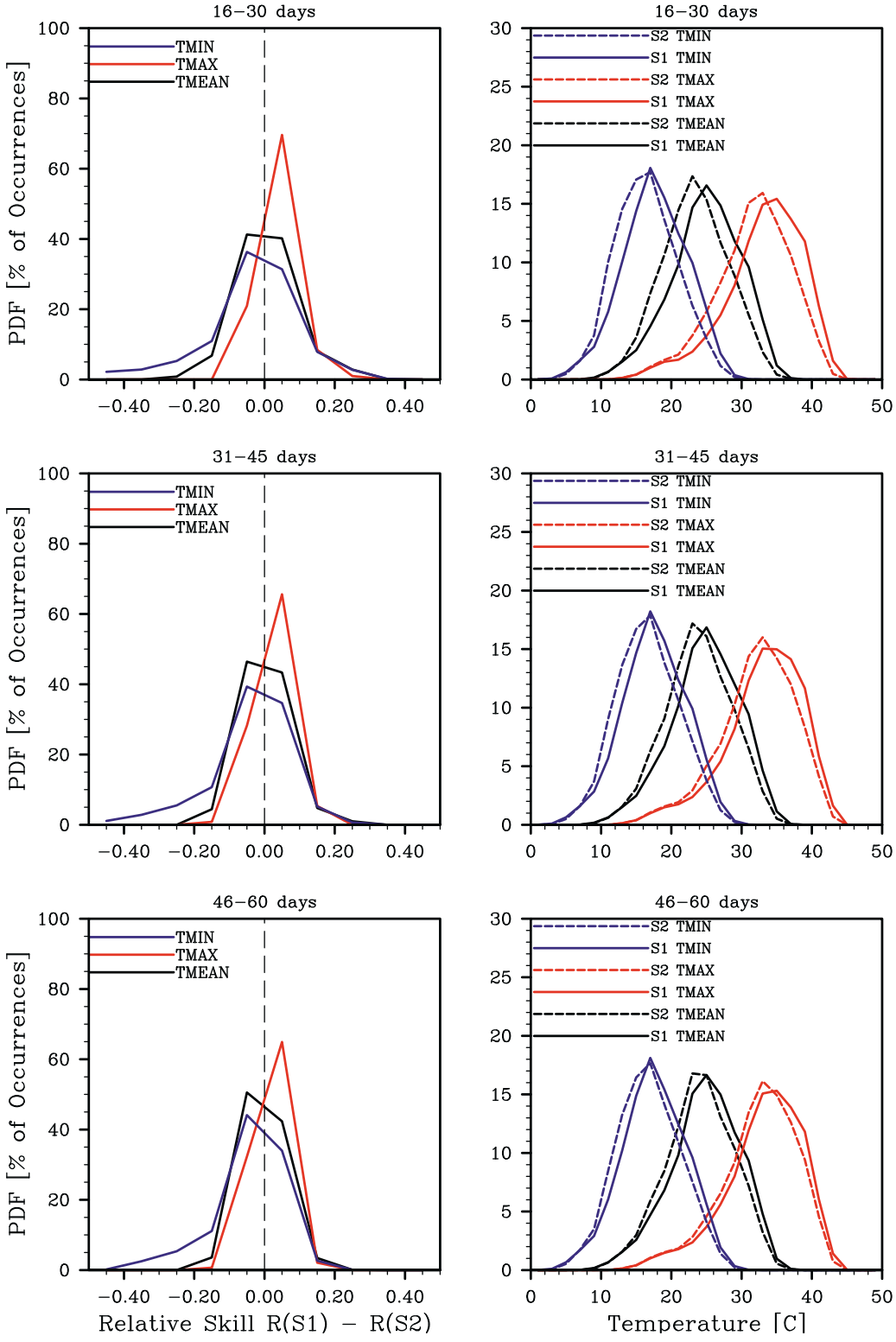

FIG. 6. (left) PDFs, expressed as percentages, of the relative change in forecast skill between S1 and S2 for mean temperature (black), maximum temperatures (red), and minimum temperatures (blue) for three different lead times: (top) 16–30, (middle) 31–45, and (bottom) 46–60 days. (right) Corresponding temperature (°C) PDFs for S1 (solid lines) and S2 (dashed lines).

TABLE 1. Percentage of the area under the temperature PDF in Fig. 6 (left) that corresponds to positive relative changes in forecast skill.

Variable	16–30 days	31–45 days	46–60 days
Mean temperature	51	49	46
Maximum temperature	79	71	67
Minimum temperature	42	41	37

The results for precipitation (Fig. 7) display limited regions where the impact of the land surface initialization on forecast skill was significant. We examined the resolution dependence of this result by aggregating our results to a resolution comparable to Koster et al. (2010), but we found there was no preferred land surface initialization method for precipitation forecast skill.

b. *Extreme soil moisture initialization and relative forecast skill*

The effect of the magnitude of the initial soil moisture anomaly on the relative change in forecast skill was assessed. We apply the same diagnostic to samples of the 100 start dates corresponding to the S1 initial soil moisture anomaly. Given that maximum temperatures had the clearest results, we only present the results for relative forecast skill associated with extreme soil moisture

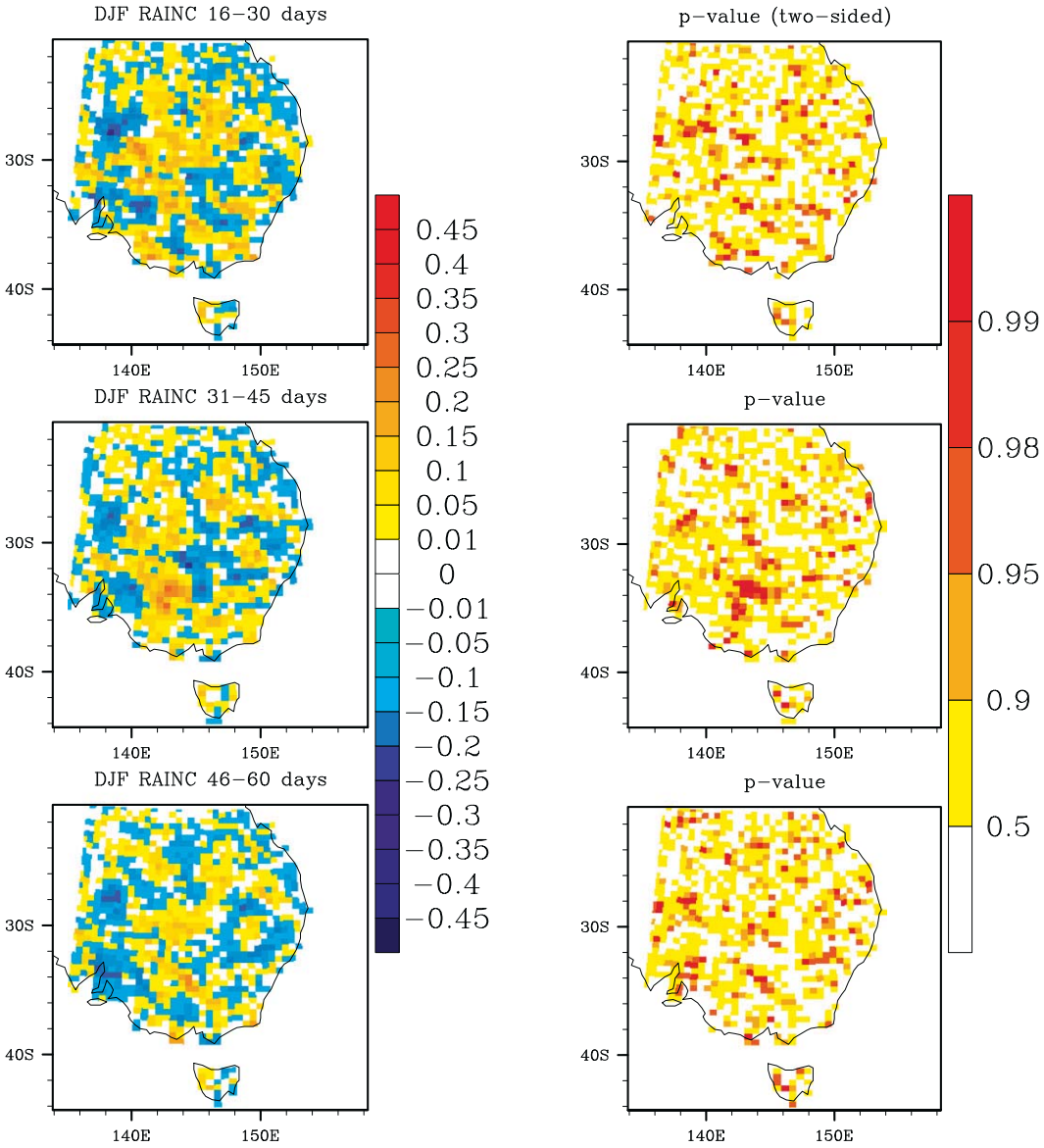

FIG. 7. As in Fig. 2, but for precipitation.

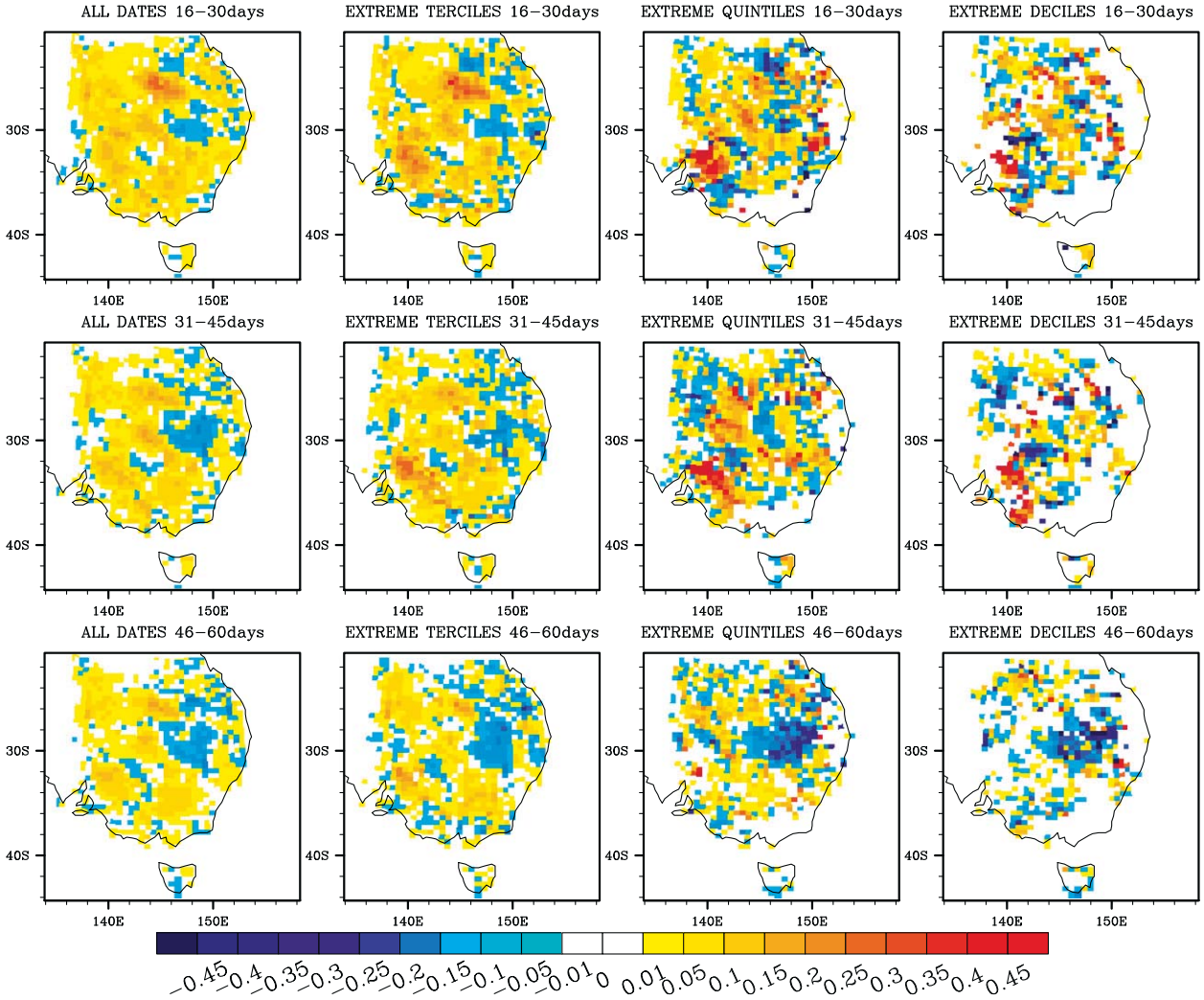

FIG. 8. (left to right) Relative gain in forecast skill for maximum 2-m air temperature, relative gain in forecast skill corresponding to the start dates initialized with soil moisture content more extreme than the upper or lower terciles, relative gain in forecast skill for extreme upper and lower quintiles, and relative gain in forecast skill for extreme upper and lower deciles for three different lead times: (top) 16–30, (middle) 31–45, and (bottom) 46–60 days.

initialization for maximum temperature (Figs. 8, 9). There is a tendency for the relative change in forecast skill to increase in absolute magnitude, whether positive or negative, with more extreme initial soil moisture anomalies (Fig. 8). The relative change in forecast skill for the extreme terciles (Fig. 8, second column) show two regions where the S1 skill exceeds S2 skill by approximately 20% (5% more than those observed using all start dates). For the extreme quintiles, there are isolated regions where the S1 skill exceeds S2 by 30%, although for the 46–60-day lead time, there is a large region where there is a decrease in S1 skill relative to S2 of 15% that is greater than the relative loss observed when using all dates. For the extreme deciles, there are less data points available to construct relative skill with less coherent change in skill across the domain. However, only the relative gains observed in Fig. 8 for the extreme terciles contain regions where the relative gain in S1 skill is statistically significant. Some of these statistically significant regions correspond to those in Fig. 9 (left column) for all dates. For the extreme quintiles and deciles (Fig. 9, right two columns), there are no regions that are statistically significant corresponding to those regions where there were more extreme changes in relative forecast skill. However, this is more likely due to the smaller sample size limiting the ability to evaluate statistical significance.

We considered whether the relative change in forecast skill had a dependency on wet or dry soil moisture anomaly initialization as opposed to extreme soil moisture initialization, where we differentiate between these

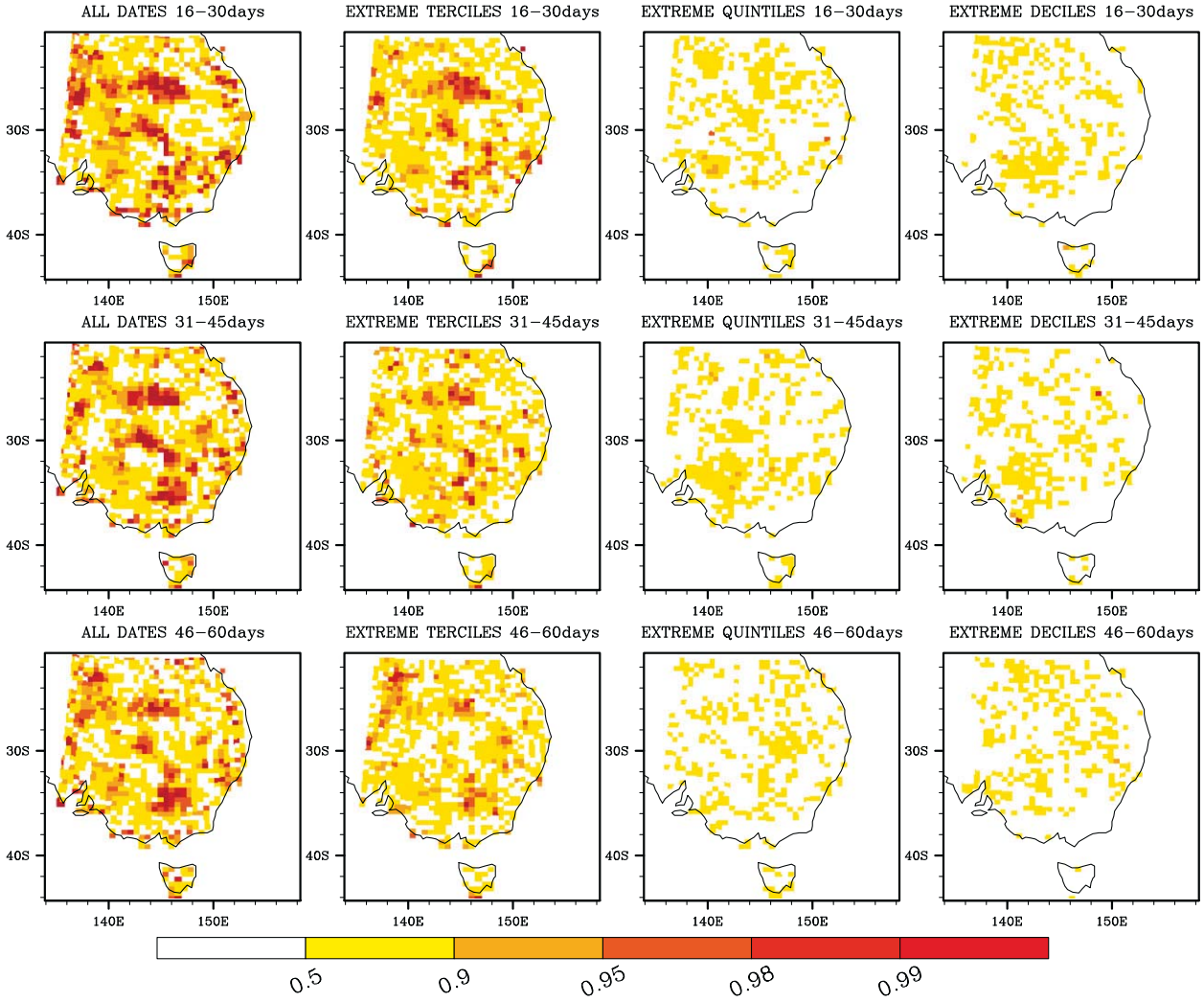

FIG. 9. As in Fig. 8, but for corresponding p values.

two classifications according to whether the initial soil moisture anomaly was positive (wet) or negative (dry). There was limited differentiation of the relative change in forecast skill between the wet and dry cases for precipitation, mean temperature, and minimum temperature. For maximum temperature (Figs. 10, 11), the dry case (Fig. 10, right) closely resembles the relative change in forecast skill derived from that using all dates (Fig. 3, left) with relative S1 gains of 10%–15% across most of the domain for all lead times. The regions with larger relative gains for S1 forecast skill are statistically significant across all lead times (Fig. 11, right). For the wet case (Fig. 10, left), there are some regions with S1 exceeding S2 skill by 30% up to 31–45 days into the forecast period. At 46–60 days, S2 skill exceeds S1 by 20% across almost half the domain; however, this is not statistically significant (Fig. 11, left). In fact, there are no regions for the wet case where the relative change in forecast skill is statistically significant. Again, this is likely associated with the sample size, where there were more extreme dry cases than wet cases, and may only be particular to the 10-yr period that the simulations cover.

c. *Comparison of forecast skill across all start dates*

To capture whether the relative change in skill is the same across all 10 start dates, rather than just those corresponding to DJF, we plot the areal average of the squared correlations (R^2) corresponding to the 16–30-, 31–45-, and 46–60-day lead times for each start date and series (Fig. 12). For precipitation (Fig. 12a) there is no clear differentiation between S1 and S2. This is consistent with Fig. 7, which showed no clear preference for land surface initialization method across the lead times. Note, in relation to Fig. 12a, R^2 values of ~0.5 can be

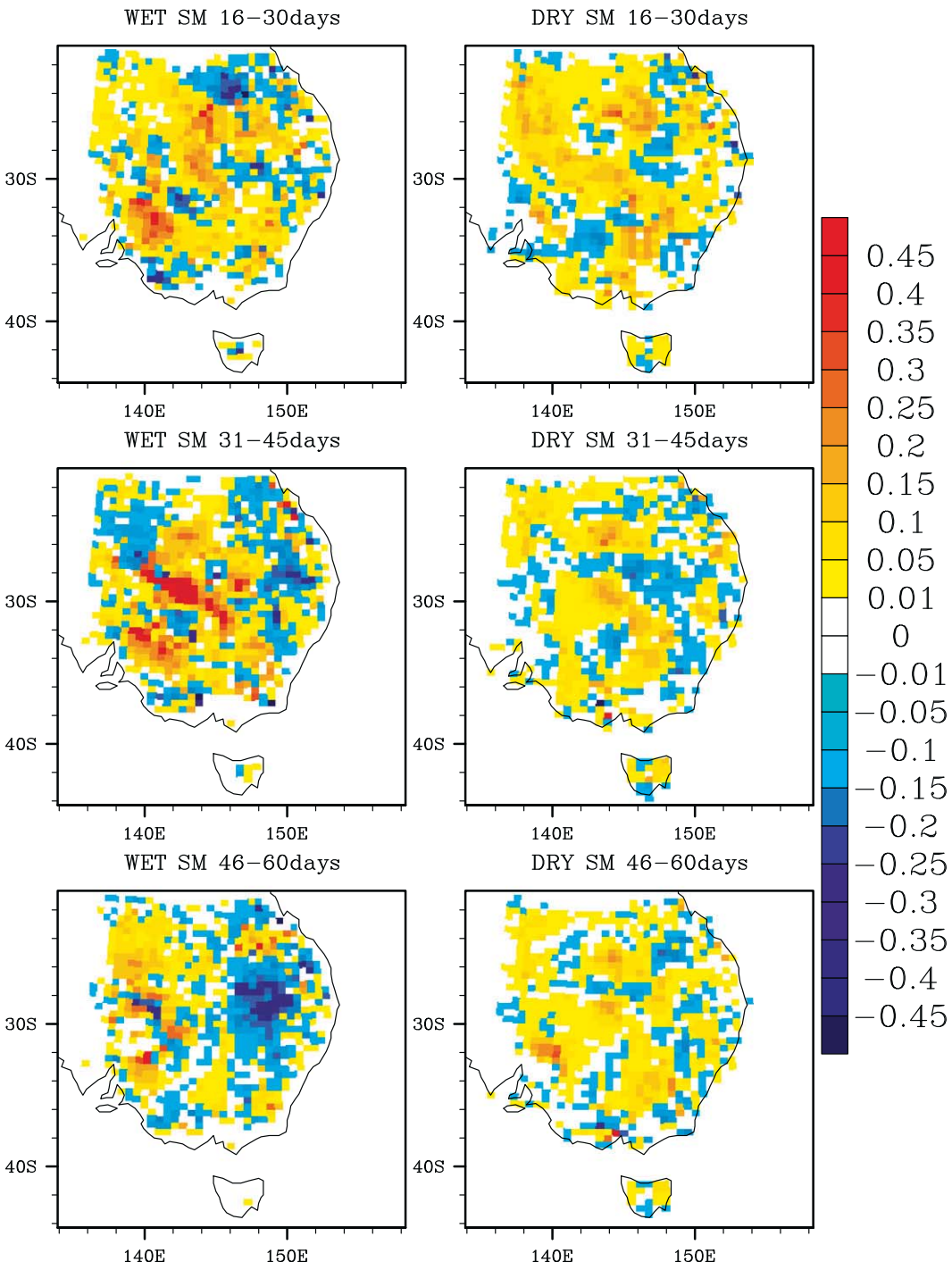

FIG. 10. Relative gain in forecast skill between S1 and S2 for start dates initialized with a (left) wet and (right) dry soil moisture anomaly for maximum 2-m air temperature for three different lead times: (top) 16–30, (middle) 31–45, and (bottom) 46–60 days.

considered high and a likely response to the lateral boundary forcing. However, these values are not indicative of the forecast skill attainable at longer lead times, with some start dates indicating that the skill at the 46–60-day lead time is less than the skill at the 31–45-day lead time. Similarly for the mean, maximum, and minimum air temperatures, there is limited differentiation between S1 and S2, although for maximum temperatures

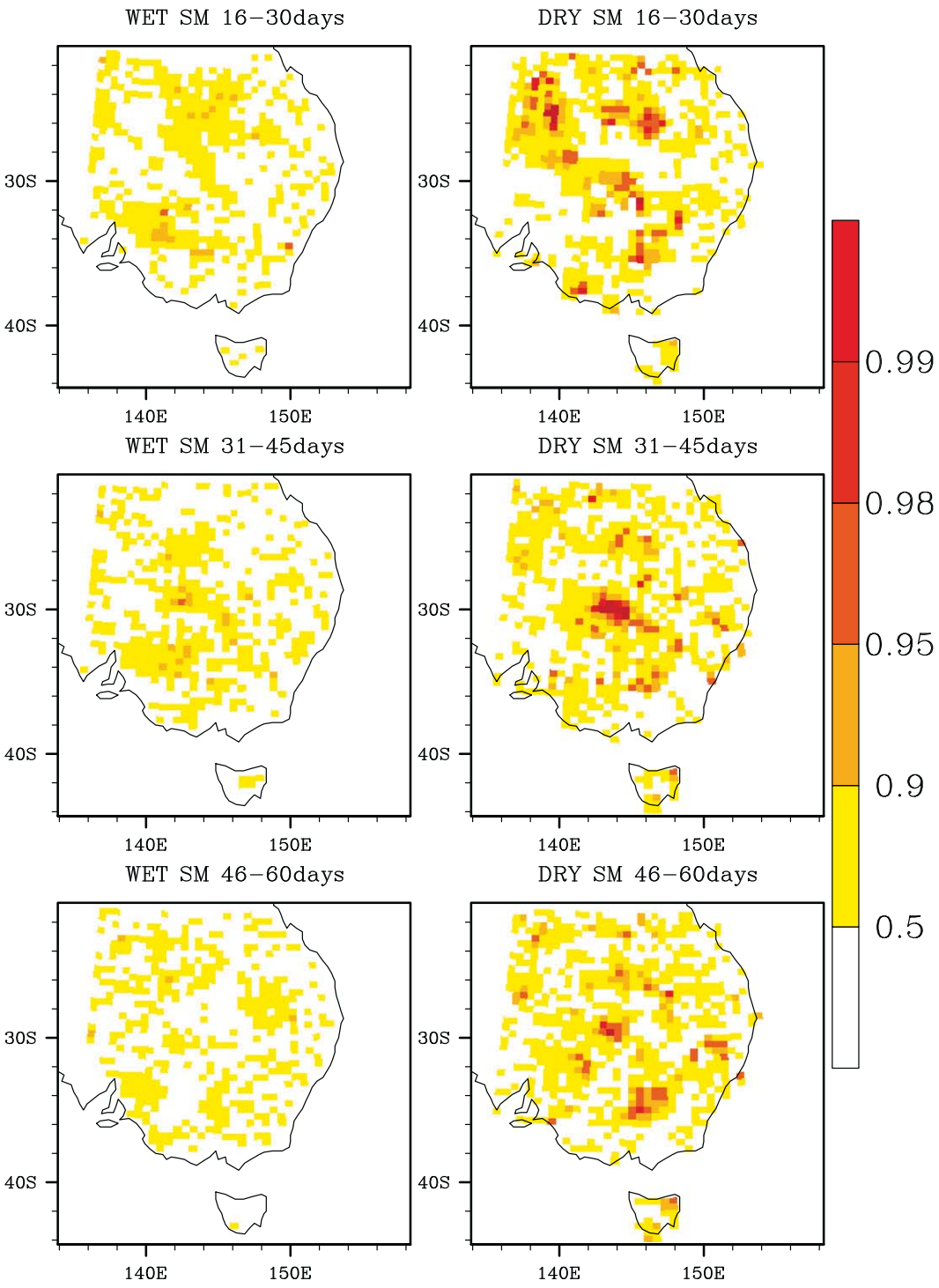

FIG. 11. As in Fig. 10, but for corresponding p values.

(Fig. 12c) S1 R^2 exceeds S2 R^2 for all start dates and lead times, consistent with the relative gain in S1 forecast skill shown in Fig. 3. For all variables in Fig. 12, the R^2 for both series are variable across the start dates, suggesting some dependence upon the initial conditions at the beginning of each forecast. There is a contrast in the R^2 values between precipitation and temperature. For precipitation R^2 values range between 0.30 and 0.50, with

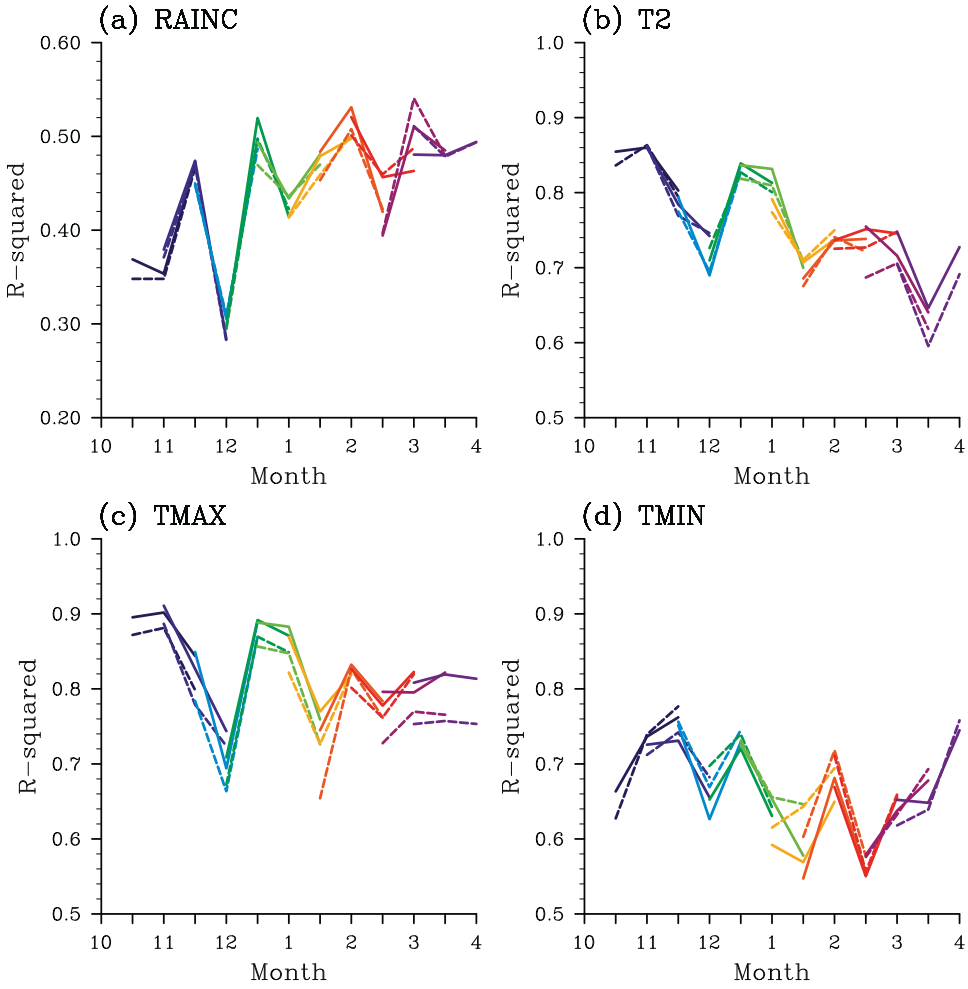

FIG. 12. Time series of the squared correlations between WRF–LIS–CABLE with AWAP as the reference truth, corresponding to each of the 10 start dates for (a) precipitation, (b) mean air temperature, (c) maximum air temperature, and (d) minimum air temperature for S1 (solid lines) and S2 (dashed lines). Colors correspond to each start date: 1 Oct, dark blue; 15 Oct, blue; 1 Nov, light blue; 15 Nov, dark green; 1 Dec, light green; 15 Dec, yellow; 1 Jan, orange; 15 Jan, red; 1 Feb, violet; and 15 Feb, dark purple.

higher values for the latter half of start dates. For mean temperature, R^2 values are between 0.60 and 0.90. The R^2 values for maximum temperature are within 0.70 and 0.90 and minimum temperature values are within 0.60 and 0.75, contributing to lower values in mean temperature, particularly for start dates corresponding to late summer and early autumn.

The potential predictability is defined as the squared correlation between the model data with the ensemble mean as the reference truth (Koster et al. 2010; van den Hurk et al. 2012), and it provides a measure of the maximum possible skill of the model system. Again, we plot the areal average for both series for all lead times and across each start date (Fig. 13). For all variables, S1 skill exceeds S2, particularly for mean and maximum temperatures, illustrating that S1 has increased internally consistency compared to S2.

4. Discussion

Our results show that subseasonal forecast skill in a regional climate model is sensitive to the land surface initialization method. In particular, temperature forecasts show relative gains in forecast skill with initialization from prior offline simulations (S1), with the greatest impact at shorter lead times of 16–30 days. The finer-scale resolution of our simulations reveals greater spatial variability in the impact of land surface initialization, with some regions showing a decrease of skill. At longer lead times, the magnitude of both positive and negative

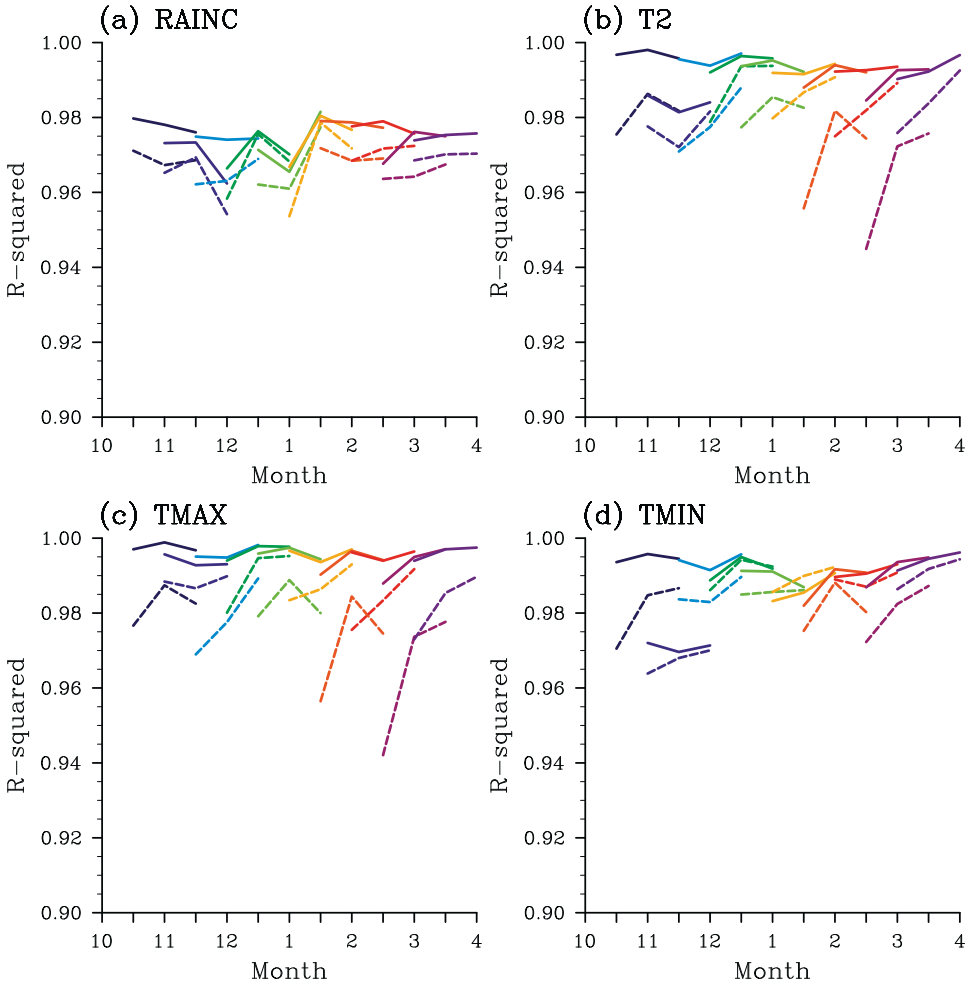

FIG. 13. As in Fig. 12, but for the time series of the potential predictability, squared correlations between WRF–LIS–CABLE with the ensemble mean as the reference truth.

relative skill decrease, showing that as the model integrates forwards in time, the simulations converge.

The distinct regions of gains and losses in skill for mean temperature were separated into maximum and minimum temperatures. These show that using offline simulations for land surface initialization is particularly important for forecasting maximum temperatures with coherent gains across the domain that were maintained 46–60 days into the forecast. The relative loss in S1 skill for mean temperature across a large proportion of the domain was associated with significant decreases in S1 skill for minimum temperature over corresponding regions. These negative skill contributions indicate that there are circumstances where using reanalyses to initialize the land surface can perform better for some variables than using prior offline simulations.

Our result for minimum temperature was associated with differences in the net longwave radiation between the two series, particularly the outgoing longwave radiation, which is largely determined by cloud cover. Differences in net shortwave radiation were smaller and did not correspond to the regions where the relative forecast skill for minimum temperature was significantly negative. A new result in this paper is the asymmetry in the coupling of soil moisture with maximum temperatures, as distinct from minimum temperatures. This asymmetry has been observed before with the impact of land cover change (Avila et al. 2012) and with the response to increases in radiative forcing (Caesar et al. 2006; Alexander et al. 2006). In our experiments, the asymmetry is relatively straightforward to explain. Soil moisture affects the partitioning of net radiation between sensible and latent heat (Seneviratne et al. 2010). During the day net radiation is dominated by solar radiation. When latent heat is dominant, because soil moisture is available, the boundary layer tends to be

cooler, shallower, and moister. When sensible heat is dominant because soil moisture is limited, a dryer, deeper, and warmer boundary layer is more common (Betts 2009). Thus, during the day there are multiple mechanisms that translate a change in soil moisture (or an availability of soil moisture) into an impact on how net radiation is partitioned and thereby into an impact on maximum temperatures. In contrast, at night, net radiation is dominated by the net exchange of longwave radiation. Minimum temperatures tend to require clear sky conditions at night that enable strong net emissions of longwave radiation. Residual heating from the surface through the soil heat flux is another component of the surface energy balance that can impart a significant influence on nighttime temperatures. Differences in the soil temperature, arising from the different initialization methods, may have contributed to the negative relative S1 skill values for minimum temperatures. In general, there is negligible coupling between the actual soil moisture and cloud cover at night, and therefore. a strong impact between soil moisture initialization and minimum temperature is less likely. However, the potential for coupling between soil temperature and minimum temperatures through the soil heat flux may explain the negative relative S1 skill values for minimum temperatures associated with the differences in soil temperature initialization. During the day, the soil heat flux is directed downward, with the difference in soil temperature imparting less influence on surface temperature. An asymmetry between the impact of soil moisture and soil temperature initialization on maximum and minimum temperatures is therefore the expected consequence of the different processes that link these quantities with net radiation.

For precipitation, the impact of land surface initialization is highly regionalized and there is no preferred land surface initialization method with respect to relative forecast skill. Similar results were found by Koster et al. (2010, 2011) and van den Hurk et al. (2012). Despite running the forecasts at a finer spatial scale to further resolve the geographical heterogeneity, limited gains in forecast skill for precipitation were possible from prior offline simulations. Precipitation over the domain is influenced by a range of synoptic-scale weather systems, including cold fronts and east coast lows (Risbey et al. 2009), which are defined to some extent by the lateral boundary conditions. These dominate the rainfall relative to the land surface boundary conditions, as seen in Fig. 12, with the moderate skill values of 40%–50%.

In general, both Koster et al. (2010) and van den Hurk et al. (2012) show that over time the impact of land surface initialization degrades, with the largest change in forecast skill within the first 30 days, and we observe similar behavior in our results. One expects that as the model integrates forward in time, whether one initializes the model with or without equilibrated land surface states, both cases will eventually converge. However, this has some dependency on the initial soil moisture state of the forecast, as shown in both Koster et al. (2010) and van den Hurk et al. (2012), and potentially for the model configuration employed. The extreme terciles show a similar spatial distribution in the relative forecast skill as that derived using all start dates. As one reduces the sample size to sample dates corresponding to more extreme soil moisture initialization, the impact on relative forecast skill appears to be greater. However, because of the small sample size, we are limited in evaluating the statistical significance of this result. Similarly, differences in the relative forecast skill between wet and dry soil initialization show that the initial soil moisture state can contribute to the final forecast skill. Our analysis of the forecast skill and potential predictability across all start dates, October through to April, shows that the impact of land surface initialization on relative forecast skill has some dependence on the antecedent soil moisture conditions at the initialization of the forecast.

5. Conclusions

We have used WRF coupled to CABLE to evaluate the sensitivity of simulation skill to two different initialization methods for a domain centered over southeastern Australia. Our results show that using land surface states obtained from offline simulations contribute relative gains in forecast skill for temperature of 10%–20% for the first 16–30 days of the forecast, with limited gains in relative skill for precipitation. These results are consistent with earlier studies that evaluate the importance of land surface initialization (Koster et al. 2010, 2011; van den Hurk et al. 2012). We extended the analysis to consider the asymmetry between maximum and minimum temperatures to understand the spatial variability of the mean temperature response to land surface initialization. We found that the strongest gains in relative forecast skill for land surface initialization from prior offline simulations were apparent for maximum temperature, with gains exceeding 20% in some regions at up to 60 days into the forecast. In contrast, the relative skill for minimum temperatures showed large regions where land surface initialization from prior offline simulation did not contribute to relative gains in forecast skill, with land surface initialization from reanalyses performing better. The contrasting response to land surface initialization between maximum and

minimum temperatures was associated with different soil moisture coupling mechanisms.

The results of Koster et al. (2010, 2011) and van den Hurk et al. (2012) are based on a multimodel consensus estimate. We have only run the experiment with a single model configuration, so we cannot exclude the possibility that our results are model dependent. However, we show that the land surface initialization method applied in a regional climate model can have significant implications for short-term simulations and the simulation of processes that are sensitive to the land surface state. In particular, the use of offline simulations to initialize soil moisture does improve the predictability for temperature, particularly maximum temperature.

Acknowledgments. This study was supported by the Australian Research Council Centre of Excellence for Climate System Science Grant CE110001028. The computational modeling was supported by the NCI National Facility at the ANU, Australia. Annette Hirsch was supported by an Australian Postgraduate Award and CSIRO OCE Postgraduate Top Up Scholarship. The authors thank Mark Decker for providing the bias-corrected MERRA data, Scott Sisson for advice on evaluating the statistical significance of our results, and Randal Koster and Bart van den Hurk for clarification on the GLACE-2 methodology. The authors would also like to thank the anonymous reviewers who provided constructive comments on the manuscript.

REFERENCES

Abramowitz, G., A. J. Pitman, H. Gupta, E. Kowalczyk, and Y. Wang, 2007: Systematic bias in land surface models. *J. Hydrometeor.,* **8,** 989–1001, doi:10.1175/JHM628.1.

——, R. Leuning, M. Clark, and A. J. Pitman, 2008: Evaluating the performance of land surface models. *J. Climate,* **21,** 5468–5481, doi:10.1175/2008JCLI2378.1.

Alexander, L. V., and Coauthors, 2006: Global observed changes in daily climate extremes of temperature and precipitation. *J. Geophys. Res.,* **111,** D05109, doi:10.1029/2005JD006290.

Avila, F. B., A. J. Pitman, M. G. Donat, L. V. Alexander, and G. Abramowitz, 2012: Climate model simulated changes in temperature extremes due to land cover change. *J. Geophys. Res.,* **117,** D04108, doi:10.1029/2011JD016382.

Beljaars, A. C. M., P. Viterbo, and M. J. Miller, 1996: The anomalous rainfall over the United States during July 1993: Sensitivity to land surface parameterization and soil moisture anomalies. *Mon. Wea. Rev.,* **124,** 362–383, doi:10.1175/1520-0493(1996)124<0362:TAROTU>2.0.CO;2.

Betts, A. K., 2009: Land-surface-atmosphere coupling in observations and models. *J. Adv. Model. Earth Syst.,* **1,** doi:10.3894/JAMES.2009.1.4.

Caesar, J., L. Alexander, and R. Vose, 2006: Large-scale changes in observed daily maximum and minimum temperatures: Creation and analysis of a new gridded data set. *J. Geophys. Res.,* **111,** D05101, doi:10.1029/2005JD006280.

Clapp, R. B., and G. M. Hornberger, 1978: Empirical equations for some soil hydraulic properties. *Water Resour. Res.,* **14,** 601–604, doi:10.1029/WR014i004p00601.

Cruz, F. T., A. J. Pitman, and Y. Wang, 2010: Can the stomatal response to higher atmospheric carbon dioxide explain the unusual temperatures during the 2002 Murray–Darling Basin drought. *J. Geophys. Res.,* **115,** D02101, doi:10.1029/2009JD012767.

Decker, M., A. J. Pitman, and J. P. Evans, 2013: Groundwater constraints on simulated transpiration variability over southeastern Australian forests. *J. Hydrometeor.,* **14,** 543–559, doi:10.1175/JHM-D-12-058.1.

Dee, D. P., and Coauthors, 2011: The ERA-Interim reanalysis: Configuration and performance of the data assimilation system. *Quart. J. Roy. Meteor. Soc.,* **137,** 553–597, doi:10.1002/qj.828.

de Noblet-Ducoudré, N., and Coauthors, 2012: Determining robust impacts of land-use-induced land cover changes on surface climate over North America and Eurasia: Results from the first set of LUCID experiments. *J. Climate,* **25,** 3261–3281, doi:10.1175/JCLI-D-11-00338.1.

Douville, H., 2010: Relative contribution of soil moisture and snow mass to seasonal climate predictability: A pilot study. *Climate Dyn.,* **34,** 797–818, doi:10.1007/s00382-008-0508-1.

——, and F. Chauvin, 2000: Relevance of soil moisture for seasonal climate predictions: A preliminary study. *Climate Dyn.,* **16,** 719–736, doi:10.1007/s003820000080.

Dudhia, J., 1989: Numerical study of convection observed during the winter monsoon experiment using a mesoscale two-dimensional model. *J. Atmos. Sci.,* **46,** 3077–3107, doi:10.1175/1520-0469(1989)046<3077:NSOCOD>2.0.CO;2.

Evans, J. P., and M. F. McCabe, 2010: Regional climate simulation over Australia's Murray-Darling basin: A multitemporal assessment. *J. Geophys. Res.,* **115,** D14114, doi:10.1029/2010JD013816.

——, and S. Westra, 2012: Investigating the mechanisms of diurnal rainfall variability using a regional climate model. *J. Climate,* **25,** 7232–7247, doi:10.1175/JCLI-D-11-00616.1.

——, A. J. Pitman, and F. T. Cruz, 2011: Coupled atmospheric and land surface dynamics over southeast Australia: A review, analysis and identification of future research priorities. *Int. J. Climatol.,* **31,** 1758–1772, doi:10.1002/joc.2206.

——, M. Ekström, and F. Ji, 2012: Evaluating the performance of a WRF physics ensemble over south-east Australia. *Climate Dyn.,* **39,** 1241–1258, doi:10.1007/s00382-011-1244-5.

Fennessy, M. J., and J. Shukla, 1999: Impact of initial soil wetness on seasonal atmospheric prediction. *J. Climate,* **12,** 3167–3180, doi:10.1175/1520-0442(1999)012<3167:IOISWO>2.0.CO;2.

Haverd, V., and Coauthors, 2012: Multiple observation types reduce uncertainty in Australia's terrestrial carbon and water cycles. *Biogeosci. Discuss.,* **9,** 12 181–12 258.

Hong, S. Y., Y. Noh, and J. Dudhia, 2006: A new vertical diffusion package with an explicit treatment of entrainment processes. *Mon. Wea. Rev.,* **134,** 2318–2341, doi:10.1175/MWR3199.1.

Jaeger, E. B., and S. I. Seneviratne, 2011: Impact of soil moisture–atmosphere coupling on European climate extremes and trends in a regional climate model. *Climate Dyn.,* **36,** 1919–1939, doi:10.1007/s00382-010-0780-8.

Jones, D., W. Wang, and R. Fawcett, 2009: High-quality spatial climate data-sets for Australia. *Aust. Meteor. Mag.,* **58,** 233–248.

Kain, J. S., 2004: The Kain–Fritsch convective parameterization: An update. *J. Appl. Meteor.,* **43,** 170–181, doi:10.1175/1520-0450(2004)043<0170:TKCPAU>2.0.CO;2.

——, and J. M. Fritsch, 1990: A one-dimensional entraining detraining plume model and its application in convective parameterization. *J. Atmos. Sci.,* **47,** 2784–2802, doi:10.1175/1520-0469(1990)047<2784:AODEPM>2.0.CO;2.

——, and ——, 1993: Convective parameterization for mesoscale models: The Kain–Fritsch scheme. *The Representation of Cumulus Convection in Numerical Models, Meteor. Monogr.,* No. 46, Amer. Meteor. Soc., 165–170.

King, A. D., L. V. Alexander, and M. G. Donat, 2013: The efficacy of using gridded data to examine extreme rainfall characteristics: A case study for Australia. *Int. J. Climatol.,* **33,** 2376–2387, doi: 10.1002/joc.3588.

Koster, R. D., and Coauthors, 2006: GLACE: The Global Land–Atmosphere Coupling Experiment. Part I: Overview. *J. Hydrometeor.,* **7,** 590–610, doi:10.1175/JHM510.1.

——, Z. Guo, R. Yang, P. A. Dirmeyer, K. Mitchell, and M. J. Puma, 2009: On the nature of soil moisture in land surface models. *J. Climate,* **22,** 4322–4335, doi:10.1175/2009JCLI2832.1.

——, and Coauthors, 2010: Contribution of land surface initialization to subseasonal forecast skill: First results from a multi-model experiment. *Geophys. Res. Lett.,* **37,** L02402, doi:10.1029/2009GL041677.

——, and Coauthors, 2011: The second phase of the Global Land–Atmosphere Coupling Experiment: Soil moisture contributions to subseasonal forecast skill. *J. Hydrometeor.,* **12,** 805–822, doi:10.1175/2011JHM1365.1.

Kowalczyk, E. A., and Coauthors, 2013: The land surface model component of ACCESS: Description and impact on the simulated surface climatology. *Aust. Meteor. Oceanogr. J.,* **63,** 65–82.

Kumar, S. V., and Coauthors, 2006: Land information system: An inter-operable framework for high resolution land surface modeling. *Environ. Model. Software,* **21,** 1402–1415, doi:10.1016/j.envsoft.2005.07.004.

Mlawer, E. J., S. J. Taubman, P. D. Brown, M. J. Lacono, and S. A. Clough, 1997: Radiative transfer for inhomogeneous atmosphere: RRTM, a validated correlated-k model for the longwave. *J. Geophys. Res.,* **102** (D14), 16 663–16 682, doi:10.1029/97JD00237.

Peters-Lidard, C. D., and Coauthors, 2007: High-performance earth system modeling with NASA/GSFC's land information system. *Innovations Syst. Software Eng.,* **3,** 157–165, doi:10.1007/s11334-007-0028-x.

Pitman, A. J., F. B. Avila, G. Abramowitz, Y. P. Wang, S. J. Phipps, and N. de Noblet-Ducoudré, 2011: Importance of background climate in determining impact of land–cover change on regional climate. *Nat. Climate Change,* **1,** 472–475, doi:10.1038/nclimate1294.

Raupach, M. R., K. Finkele, and L. Zhang, 1997: SCAM (Soil-Canopy-Atmosphere Model): Description and comparison with field data. Tech. Rep. 132, CSIRO Centre for Environmental Mechanics, Canberra, ACT, Australia, 81 pp.

Reichle, R. H., R. D. Koster, G. J. M. de Lannoy, B. A. Forman, Q. Liu, S. P. P. Mahanama, and A. Tourè, 2011: Assessment and enhancement of MERRA land surface hydrology estimates. *J. Climate,* **24,** 6322–6338, doi:10.1175/JCLI-D-10-05033.1.

Risbey, J. S., M. J. Pook, P. C. McIntosh, M. C. Wheeler, and H. H. Hendon, 2009: On the remote drivers of rainfall variability in Australia. *Mon. Wea. Rev.,* **137,** 3233–3253, doi:10.1175/2009MWR2861.1.

Santanello, J. A., C. D. Peters-Lidard, and S. V. Kumar, 2011: Diagnosing the sensitivity of local land–atmosphere coupling via the soil moisture–boundary layer interaction. *J. Hydrometeor.,* **12,** 766–786, doi:10.1175/JHM-D-10-05014.1.

——, ——, A. Kennedy, and S. V. Kumar, 2013: Diagnosing the nature of land–atmosphere coupling: A case study of dry/wet extremes in the U.S. southern Great Plains. *J. Hydrometeor.,* **14,** 3–24, doi:10.1175/JHM-D-12-023.1.

Seneviratne, S. I., T. Corti, E. L. Davin, M. Hirschi, E. B. Jaeger, I. Lehner, B. Orlowsky, and A. J. Teuling, 2010: Investigating soil moisture–climate interactions in a changing climate: A review. *Earth Sci. Rev.,* **99,** 125–161, doi:10.1016/j.earscirev.2010.02.004.

Skamarock, W. C., and Coauthors, 2008: A description of the Advanced Research WRF version 3. NCAR Tech. Note NCAR/TN-475+STR, 113 pp. [Available online at http://www.mmm.ucar.edu/wrf/users/docs/arw_v3.pdf.]

Timbal, B., S. Power, R. Colman, J. Viviand, and S. Lirola, 2002: Does soil moisture influence climate variability and predictability over Australia? *J. Climate,* **15,** 1230–1238, doi:10.1175/1520-0442(2002)015<1230:DSMICV>2.0.CO;2.

van den Hurk, B., F. Doblas-Reyes, G. Balsamo, R. D. Koster, S. I. Seneviratne, and H. Camargo Jr., 2012: Soil moisture effects on seasonal temperature and precipitation forecast scores in Europe. *Climate Dyn.,* **38,** 349–362, doi:10.1007/s00382-010-0956-2.

Wang, Y. P., E. Kowalczyk, R. Leuning, G. Abramowitz, M. R. Raupach, B. Pak, E. van Gorsel, and A. Luhar, 2011: Diagnosing errors in a land surface model (CABLE) in the time and frequency domains. *J. Geophys. Res.,* **116,** G01034, doi:10.1029/2010JG001385.

Zhang, Q., Y. P. Wang, A. J. Pitman, and Y. J. Dai, 2011: Limitations of nitrogen and phosphorous on the terrestrial carbon uptake in the 20th century. *Geophys. Res. Lett.,* **38,** L22701, doi:10.1029/2011GL049244.